Biocatalysis and Biotransformation

ISSN: (Print) (Online) Journal homepage: https://www.tandfonline.com/loi/ibab20

Biochemical and biophysical characterisation of a small purified lipase from *Rhizopus oryzae* ZAC3

Zainab A. Ayinla, Adedeji N. Ademakinwa, Richard A. Gross & Femi K. Agboola

To cite this article: Zainab A. Ayinla, Adedeji N. Ademakinwa, Richard A. Gross & Femi K. Agboola (2021): Biochemical and biophysical characterisation of a small purified lipase from *Rhizopus oryzae* ZAC3, Biocatalysis and Biotransformation, DOI: 10.1080/10242422.2021.1883006

To link to this article: https://doi.org/10.1080/10242422.2021.1883006

Published online: 08 Feb 2021.

BIOCATALYSIS AND BIOTRANSFORMATION
https://doi.org/10.1080/10242422.2021.1883006

Taylor & Francis
Taylor & Francis Group

RESEARCH ARTICLE

Biochemical and biophysical characterisation of a small purified lipase from *Rhizopus oryzae* ZAC3

Zainab A. Ayinla[a], Adedeji N. Ademakinwa[a], Richard A. Gross[b] and Femi K. Agboola[a]

[a]Department of Biochemistry and Molecular Biology, Obafemi Awolowo University, Ile-Ife, Nigeria; [b]Center for Biotechnology and Interdisciplinary Studies, Rensselaer Polytechnic Institute, Troy, NY, USA

ABSTRACT

The characteristics of a purified lipase from *Rhizopus oryzae* ZAC3 (*Ro*L-ZAC3) were investigated. *Ro*L-ZAC3, a 15.8 kDa protein, which was optimally active at pH 8 and 55 °C had a half-life of 126 min at 60 °C. The kinetic parameters using *p*-nitrophenylbutyrate as substrate were 0.19 ± 0.02 mM, 126 ± 5.6 U/ml and 122 s^{-1} for K_m, V_{max} and k_{cat} respectively. *Ro*L-ZAC3 showed stability in methanol and isopropanol with Na^+ enhancing the activity. *p*-nitrophenyloleate and castor oil were the best preferred substrates among the *p*-nitrophenyl esters and vegetable oils tested respectively. About 43% residual activity was observed after incubation for 30 min at 75 °C. Circular dichroism thermal scan showed that the lipase displayed intense negative ellipticities even at high temperature. Perturbation of the tertiary structure with increasing temperature caused the exposure of hydrophobic side chains to the aqueous environment as revealed by tryptophan fluorescence, with a $t-T_m$ of 50 °C. Differential scanning calorimetry analysis showed melting temperature and calorimetric enthalpy of 55.5 °C and 444 kJ/mol respectively. Dynamic light scattering analysis indicated that the lipase was prone to aggregation upon unfolding at high temperature. It can be concluded that *Ro*L-ZAC3 possesses promising potential for numerous biotechnological applications.

ARTICLE HISTORY
Received 25 November 2020
Revised 24 January 2021
Accepted 25 January 2021

KEYWORDS
Lipase; *Rhizopus oryzae*; tryptophan fluorescence; circular dichroism; calorimetric enthalpy

Introduction

Knowledge of how surrounding environmental factors such as ionic strength, temperature, solvent composition and pH influence structure-function relationship in terms of folding and stability is crucial for improved enzyme production at the industrial scale and for theoretical purpose, as such knowledge provides an insight into the molecular basis of enzyme stability (Kishore et al. 2012). Thus, pH denaturation, chemical unfolding with the use of chaotropic agents (such as guanidinium chloride and urea) and thermal denaturation can be used for measuring conformational stability and enzymatic activity (Rabbani et al. 2012).

Lipases (triacylglycerol acyl hydrolases) speed up the breakdown of triglycerides at the lipid-water interface and also catalyse the reverse reactions, which include triglyceride synthesis, esterification, interesterification, transesterification, aminolysis, acidolysis and alcoholysis (Salihu and Alam 2012). Catalysis by these hydrolases occurs in biphasic (polar/non-polar) media, in which the polar component solubilises the enzyme while the non-polar component solubilises the substrates. Fungal lipases generally have molecular weights ranging from less than 20 kDa–60 kDa (Mehta et al. 2017). Only very few reports exist on small lipases with molecular weights less than 20 kDa. These include lipases from microbial strains such as *Rhizopus* strain JK-1, 16.25 kDa (Kantak and Prabhune 2012), *Rhizopus arrhizus,* 6.9 kDa (Dobrev et al. 2011), *Bacillus thermoleovorans* CCR11, 11 kDa (Castro-Ochoa et al. 2005), *Fusarium* sp. YM-30, 12 kDa (Mase et al. 1995) and *Bacillus thermoleovorans* ID-1, 18 kDa (Lee et al. 2001). There are even fewer studies on their complete purification and characterisation, particularly for fungal lipases and specifically even less common for *Rhizopus* sp. Generally, the low molecular weight property endows such enzymes with industrial potential and can easily be exploited for better and wider substrate specificity because the amino acids are relatively easy to modify (Kantak and Prabhune 2012), unlike the modification of larger proteins in which the possibilities of side products and missed modifications increase with increasing protein size. Also, complete modification of large proteins may present difficulties

CONTACT Femi K. Agboola fkagbo@oauife.edu.ng Department of Biochemistry and Molecular Biology, Obafemi Awolowo University, Ile-Ife, Nigeria

due to the increased chances of higher order structure and incomplete denaturation (Krusemark et al. 2011).

Previous work reported the isolation of the fungus, *Rhizopus oryzae* ZAC3 (*Ro*ZAC3), and the enzyme production under optimised conditions (Ayinla et al. 2017). This study aims at understanding the stability and conformational dynamics of the low molecular weight *Rhizopus oryzae* ZAC3 lipase (*Ro*L-ZAC3). In this study, we report the physicochemical properties, as well as the structural features (folding/unfolding studies) of *Ro*L-ZAC3. Changes in conformation and stability were assessed by far ultraviolet-circular dichroism (CD), differential scanning calorimetry (DSC), fluorescence spectroscopy and dynamic light scattering (DLS). Far-UV CD was used to study changes in *Ro*L-ZAC3 secondary structure at different temperature, pH and guanidinium chloride (Gdm-Cl) concentration. The tertiary structure of the protein was studied by fluorescence spectroscopy while data for tertiary structure melting temperature ($t - T_m$), calorimetric enthalpy (ΔH_{cal}) and the changes in excess heat capacity (ΔC_p) were obtained from DSC measurements.

Materials and methods

Materials

p-nitrophenyl acetate (*p*NPA), *p*-nitrophenyl butyrate (*p*NPB), *p*-nitrophenyl laurate (*p*NPL), *p*-nitrophenyl palmitate (*p*NPP), *p*-nitrophenyl oleate (*p*NPO), triton X-100, isopropanol, sodium dihydrogen phosphate and disodium hydrogen phosphate were purchased from Sigma-Aldrich (St. Louis, USA). SimplyBlue™ Safe Stain (Coomassie G-250) and Pierce™ BCA (bicinchoninic acid) protein assay kit were obtained from ThermoFisher Scientific™ (Massachusetts, USA). Bio-Rad Precision Plus Protein Standards was from Bio-Rad (Hercules, USA). All the chemicals and reagents used were of analytical grade.

Lipase activity assay

Lipase activity was assayed spectrophotometrically using *p*-NPB as substrate according to the method of Vorderwulbecke et al. (1992) with slight modification. One hundred microlitres of the enzyme solution was added to 900 µL of 50 mM sodium phosphate buffer, pH 8 (containing 1% Triton X-100). The assay was initiated by the addition of 30 µL of *p*NPB solution (14 mM in isopropanol) to the diluted enzyme solution. The absorbance at 405 nm was monitored over 3 min in a spectrophotometer. The initial reaction rate was then determined from the linear plot. One unit (1 U) of *Ro*L-ZAC3 activity was the amount of enzyme that released 1 µmol of *p*-nitrophenol from *p*-NPB in one minute under the assay conditions.

Production, purification and molecular weight determination of RoL-ZAC3

R. oryzae ZAC3 lipase (*Ro*L-ZAC3), an extracellular enzyme, was produced by submerged fermentation (in medium containing 1% olive oil, 1% xylose, 1% yeast extract at pH 5 and temperature of 45 °C for 96 h) as previously reported (Ayinla et al. 2017). The crude enzyme was concentrated by ultrafiltration and loaded onto a pre-equilibrated DEAE–Sepharose column (0.5 cm × 9.6 cm) on an AKTA FPLC system from GE Healthcare at 4 °C. After successive washes with the equilibration buffer (50 mM sodium phosphate buffer, pH 8), bound proteins were eluted with the same buffer using a linear gradient of $0.5 - 1$ M NaCl. Elution was at a flow rate of 1.9 ml/min and monitored by absorbance at 280 nm. Peak fractions were assayed for lipase activity and active fractions were pooled.

Gel filtration on Sephacryl S-200 column (1.6 cm × 60 cm) was used to determine the native molecular weight of *Ro*L-ZAC3. The column was calibrated with the following protein standards of different molecular weights: bovine serum albumin (66,000 Da), ovalbumin (45,000 Da), pepsin (35,000 Da), trypsin (24,000 Da) and lysozyme (14,000 Da). The purity and subunit molecular weight was ascertained on 15% sodium dodecyl sulfate-polyacrylamide gel electrophoresis (SDS-PAGE) as described by Laemmli (1970). Protein concentrations were determined by the method of Smith et al. (1985) using the BCA protein assay kit.

Effect of temperature on RoL-ZAC3 activity and stability

The optimal temperature for the purified lipase was determined by heating the appropriately diluted enzyme at a specific temperature (ranging from 15 °C to 85 °C respectively) for 5 min in an Eppendorf thermomixer®, followed by the addition of the *p*NPB substrate and determining the lipase activity as described earlier.

The thermal stability was investigated by incubating the diluted enzyme at different temperatures (55–75 °C) for 2 h and withdrawing aliquots (1 ml) of the enzyme at 30 min intervals. The incubation was carried out in an Eppendorf Thermomixer® at a specific temperature with constant mixing at 350 rpm. The withdrawn enzyme was rapidly cooled on ice for

5 min and left at room temperature for 10 min, followed by the addition of the *p*NPB substrate solution and assayed for lipase activity. The residual activities (a measure of irreversible enzyme activity loss) were expressed as a percentage of the activity at time zero (activity when enzyme had not been heated) which was taken to be 100%. The k_d is the deactivation rate constant. The data from the thermal stability study were fit to first order deactivation kinetics and the apparent half-life values ($t_{1/2}$) estimated using $t_{1/2} = \ln 2/k_d$ (k_d = deactivation rate constant).

Effect of pH on RoL-ZAC3 activity and stability

To determine the optimum pH, lipase activity assays were carried out in the following buffers at the indicated pH values: 50 mM phosphate buffer (pH 3.0–3.5), 50 mM acetate buffer (pH 4.0–5.0), 50 mM citrate buffer (pH 5.5–6.0), 50 mM phosphate buffer (pH 6.0–8.5), 50 mM Tris buffer (pH 7.0–9.5) and 50 mM borate buffer (pH 9–9.5).

The pH stability (at pH 7, 7.5, 8 and 8.5) was determined by incubating the enzyme in phosphate buffer (50 mM, pH 7 − 8.5) for 1 h while withdrawing a 100 µL aliquot for assaying at 15 min intervals.

Kinetic studies

The apparent kinetic parameters (K_m, V_{max} and k_{cat}) of *Ro*L-ZAC3 for *p*NPB were determined by varying the concentration of *p*NPB between 0.05 and 1.0 mM. Temperature and pH were maintained at 55 °C and pH 8 respectively. The initial reaction rate was determined for each concentration of *p*NPB and the data plotted according to Lineweaver and Burk (1934) using GraphPad Prism 7. The k_{cat} was calculated by using V_{max}, molecular weight and concentration of the enzyme (0.267 mg/ml). The equation is shown as follows:

$$k_{cat} = V_{max}/[E_t]$$

where $[E_t]$ is the enzyme concentration in µM.

Effect of metal ions on RoL-ZAC3 activity

The effect of metal ions on *Ro*L-ZAC3 activity was determined by incubating 100 µL of the enzyme with 5, 10 and 20 mM of chloride salts of different metal ions (Na^+, K^+, Ca^{2+}, Ba^{2+}, Mg^{2+}, Mn^{2+} and Hg^{2+} respectively) in sodium phosphate buffer (pH 8) containing 1% triton X-100 for 1 min. Lipase activity was subsequently assayed as previously described above. The reaction in the absence of metal ions was taken as control.

Effect of organic solvents on RoL-ZAC3 activity

To determine the effect of organic solvents on *Ro*L-ZAC3 activity, reaction was performed in the presence of 20% organic solvents with different polarities (log*p* values): methanol (−0.76), ethanol (−0.24), acetone (−0.23), isopropanol (0.05), t-butanol (0.58), ethylacetate (0.64), dichloromethane (1.25) and hexane (3.5). The relative activity for each organic solvent was determined as percentages of the activity obtained with isopropanol (Pimentel et al. 2007).

Substrate specificity

The effect of several substrates on *Ro*L-ZAC3 was determined using the following *p*-nitrophenyl esters (0.1% w/v) as substrates: *p*NPA, *p*NPB, *p*NPL, *p*NPP and *p*NPO. The standard protocol for *p*NPB was followed for all the other substrates using 30 µL aliquot. The relative activities were ascertained as percentages of the activity obtained with *p*NPB (Ekinci et al. 2016).

Effect of RoL-ZAC3 on natural oils

The hydrolytic activity of *Ro*L-ZAC3 on various natural oils (olive oil, castor oil, lemon oil, origanum oil) was investigated by titrimetric method. The emulsion was prepared by emulsifying 10% (v/v) oil with 5% (w/v) gum arabic in 50 mM sodium phosphate buffer, pH 7. The enzyme (100 µL) was added to the emulsion followed by incubation at 37 °C for 30 min. One millilitre of acetone: ethanol (1:1) solution was used to terminate the reaction and to extract the fatty acid. Titration with 1 M NaOH was used to estimate the amount of fatty acids liberated (Sirisha et al. 2010).

Circular dichroism (CD) analysis

A JASCO J-815 spectropolarimeter with a Peltier-type temperature controller coupled to it was used for CD analysis. The CD spectra were recorded using Spectra Manager 228 software (JASCO, Easton, USA). All recorded spectra were an average of 4 accumulations. Analysis was performed in a 1-mm pathlength cuvette using 10 µM lipase solutions prepared in (i) 10 mM sodium acetate buffer at pH 5.0 and (ii) 10 mM sodium phosphate buffer at pH 8 depending on the pH being tested. To analyse the protein secondary structure, wavelength scans were performed in the far-UV

(260–200 nm) wavelength range at a scan rate of 50 nm/min at 25 °C. Following this, CD thermal unfolding scans were performed from 10 °C to 80 °C at a scan rate of 1°Cmin^{-1}. Ellipticity (θ), expressed in mdeg by the spectropolarimeter, was converted to mean residue ellipticity, MRE ($[\theta]_{mrw}$) in deg cm^2 dmol^{-1}. Thermal denaturation of the enzyme was followed by continuously monitoring ellipticity changes at 207 nm as a function of temperature.

Guanidinium chloride (GdmCl)-induced lipase unfolding was also characterised by CD. Protein solutions (10 μM) were incubated overnight in 10 mM sodium phosphate buffer with varying concentrations of GdmCl (1, 3 and 6 M) at 25 °C. Incubating overnight was necessary to allow enough time for equilibrium between folded and unfolded states. The lipase-GdmCl solutions were then subjected to CD wavelength scans as described above and the ellipticity from 260 to 200 nm for each GdmCl concentration was recorded.

Differential scanning calorimetry (DSC) analysis

A NanoDSC differential scanning calorimeter (TA Instruments, New Castle, USA) with a sample cell volume of 300 μL was used for the calorimetric measurements of melting temperature (T_m). The enzyme sample (300 μL) was loaded into the sample capillary cell and similar volume of 10 mM sodium phosphate buffer was loaded into the reference capillary cell. The cells were heated from 20 °C to 100 °C at 3 atm pressure and a rate 1°Cmin^{-1}. The resulting thermogram was baseline corrected and NanoAnalyze software was used to analyse the normalised data. From this, estimates of the melting temperature (T_m) and denaturation enthalpy (ΔH) were determined.

Intrinsic tryptophan fluorescence analysis

Intrinsic tryptophan fluorescence analysis was performed on a Spex Fluorolog® Tau-3 (Horiba, New Jersey, USA) fluorimeter. Slit width of 3 nm was used for the excitation and emission beam. A concentration of 2 μM of the protein solution in 10 mM phosphate buffer, pH 8 was used for the analysis. Excitation was at 295 nm and intrinsic tryptophan fluorescence emission was recorded from 300 to 410 nm (wavelength scan). For the wavelength scan, a blank buffer scan was also run, which was subtracted from the protein scan. The wavelength that gave the highest fluorescence intensity, denoted λ_{max}, was obtained from the wavelength scan. A temperature scan was run for the thermal transition analysis. Temperature was increased at intervals of 5 °C and sample was incubated for 3 min at each temperature. A plot of λ_{max} as a function of temperature was made and the midpoint of this thermal transition was taken as the $t - T_m$ (protein tertiary structure melting/unfolding temperature).

Dynamic light scattering (DLS) analysis

Aggregation studies were carried out by DLS analysis to determine the temperature at which aggregates begin to form as the protein unfolds. DLS measurements were carried out on a Malvern Zetasizer ZSP90 (Malvern, Massachusetts, USA). Thermal scans were run on 10 μM protein solution from 25 °C to 90 °C at intervals of 5 °C and equilibration time of 180 s at each temperature. As the temperature increased, the scattered light intensity was measured. A sharp rise in the intensity of scattered light signified the onset/beginning of aggregation denoted T_{agg} (aggregation point) (Shirke et al. 2018).

Results

Estimation of RoL-ZAC3 molecular weight

*Ro*L-ZAC3 was purified 2.5-fold to apparent homogeneity by the process of ultrafiltration and DEAE-Sepharose anion exchange chromatography with a 47% overall recovery (Table 1). A distinct band corresponding to a subunit molecular weight of 15.8 kDa was obtained on SDS-PAGE (Figure 1). This was consistent with the native molecular weight of 16.2 kDa determined by gel filtration chromatography on Sephacryl S-200. This suggests that the lipase exists as a monomer.

Temperature effect and thermal stability of RoL-ZAC3

The effect of temperature on the lipolytic activity of *Ro*L-ZAC3 showed an optimum temperature, T_{opt} at 55 °C (Figure 2(A)). Further increase in temperature

Table 1. RoL-ZAC3 purification table.

	Total activity (U)	Total protein (mg)	Specific activity (U/mg)	Yield (%)	Purification fold
Crude	1403	21.4	65.6	100	1
Ultrafiltration	935	10.8	86.6	66.6	1.3
DEAE-Sepharose	660	4.1	161	47.0	2.5

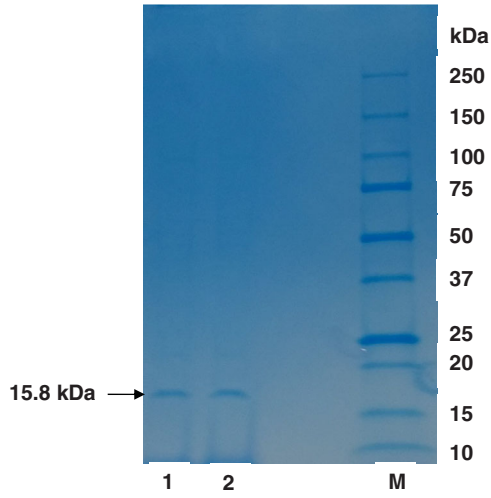

Figure 1. SDS-PAGE analysis of *Ro*L-ZAC3. Lane 1 & 2, purified *Ro*L-ZAC3; lane M, protein molecular weight markers (Precision Plus Protein™ unstained standards, BioRad).

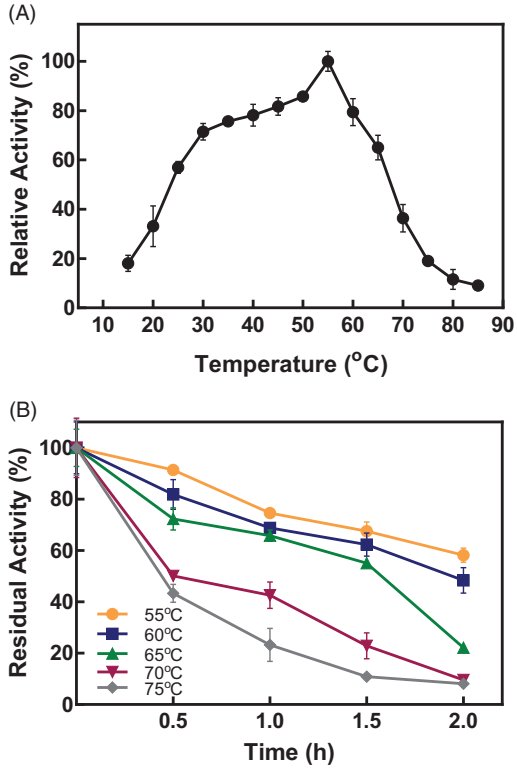

Figure 2. Effect of temperature on *Ro*L-ZAC3 activity and stability. (A) Optimal temperature. (B) Thermal stability. Error bars represent deviations from triplicate experiments. The half-life values are summarised in Table 2.

beyond 55 °C led to a decline in enzyme activity, and the enzyme almost completely lost its activity at 85 °C.

Thermostability profile of *Ro*L-ZAC3 is shown in Figure 2(B). *Ro*L-ZAC3 showed about 72% residual activity after incubation at 65 °C for 30 min. Almost 55% activity was recovered after 90 min of incubation

Table 2. Half-life (in hours) of *Ro*L-ZAC3 at different temperatures.

Temperature (°C)	Half-life, $t_{1/2}$ (h)
55	2.5
60	2.1
65	1.1
70	0.6
75	0.5

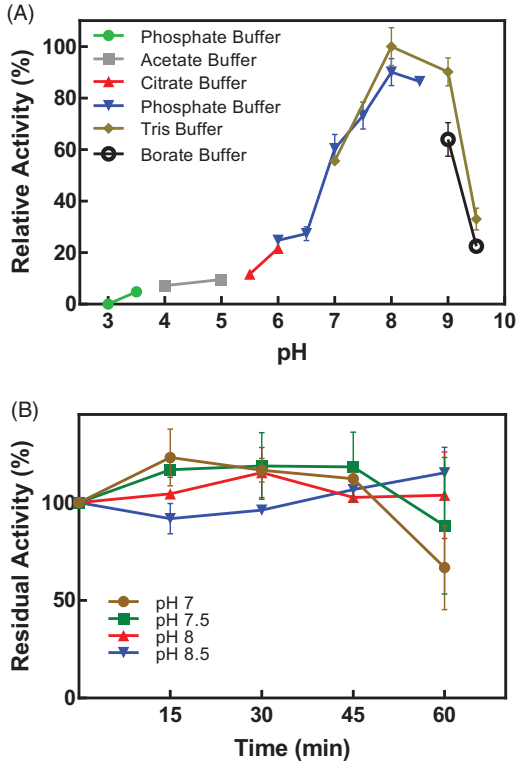

Figure 3. Effect of pH on *Ro*L-ZAC3 activity and stability. (A) Optimal pH. (B) pH stability. The values shown represent the average from triplicate experiments. Error bars represent the standard deviation.

at 65 °C and this dropped further to 22% after 120 min incubation. The apparent half-life ($t_{1/2}$) of *Ro*L-ZAC3 at different temperatures is summarised in Table 2. Plot of Ln (E_t/E_o) vs time is available in supplemental material.

pH effect and pH stability of RoL-ZAC3

*Ro*L-ZAC3 showed an optimum pH of 8 (Figure 3(A)). The broad pH optimum exhibited by the enzyme extends well into the alkaline range (7–9.5). Very low activity was seen below pH 6 and no activity was seen below pH 3.5. At pH 7.5, 8.5 and 9, relative activities were about 84%, 95% and 90% respectively. The pH stability of the enzyme was also investigated over a pH range of 7 – 8.5 (Figure 3(B)). Over 100% residual

Table 3. Summary of kinetic parameters for *Ro*L-ZAC3.

Substrate	K_m (mM)	V_{max} (U/ml)	k_{cat} (s^{-1})
*p*NPB	0.19 ± 0.02	126 ± 5.6	123

K_m: Michaelis Constant; V_{max}: maximum reaction rate; k_{cat}: turn-over number.

Table 4. Effect of metal ions on activity of *Ro*L-ZAC3.

Metal ions	5 mM	10 mM	20 mM
Na^+	137 ± 6.1	151 ± 3.3	136 ± 11.4
K^+	129 ± 30.4	107 ± 21.3	79.2 ± 1.3
Ca^{2+}	46.3 ± 2.3	81.7 ± 10.8	95.1 ± 5.8
Ba^{2+}	93.7 ± 11.0	92.6 ± 8.6	100 ± 0.9
Mg^{2+}	88.7 ± 18.1	77.9 ± 33.5	36.2 ± 1.6
Mn^{2+}	38.8 ± 0.9	17.8 ± 1.2	0
Hg^{2+}	44.6 ± 1.6	48.2 ± 0.4	52.8 ± 0.4

The chloride salt of each metal ion was added to final concentrations of 5, 10 and 20 mM prior to assay of enzyme activity. The percentage activities were determined relative to the control (without any metal ion). Values are means ± SD ($n = 3$).

activities were also observed at pH 8 and 8.5 after 30 min and 60 min incubation respectively.

Determination of kinetic parameters

The hydrolysis of *p*NPB by *Ro*L-ZAC3 followed the Michaelis-Menten kinetics. The kinetic study showed that the Michaelis-Menten constant (K_m) was 0.19 ± 0.02 mM and the hydrolysis of *p*NPB occurred at a maximum reaction rate (V_{max}) of 126 ± 5.6 U/ml of enzyme, as estimated from the Lineweaver Burk plot. The turn-over number (k_{cat}), which is a measure of the number of substrate molecules converted to product per unit time was 123 s^{-1} (Table 3).

Effect of metal ions on RoL-ZAC3 activity

*Ro*L-ZAC3 activity was inhibited by chloride salts of Mn^{2+} and Hg^{2+} even at low concentrations of 5 and 10 mM. Poor activity was also observed with Mg^{2+} at 20 mM concentration (Table 4). Mn^{2+} completely inhibited the enzyme activity at 20 mM. Of all the metal ions tested, Na^+ significantly enhanced lipase activity at all three concentrations (5, 10, 20 mM), giving percent relative activity as high as 150%. K^+ enhanced lipase activity at 5 and 10 mM but slightly inhibited the activity by about 25% at a high concentration of 20 mM. The enzyme displayed more activity at higher Ca^{2+} concentrations of 10 and 20 mM than it did at 5 mM (Table 4).

Effect of organic solvents on RoL-ZAC3 activity

In this study, the highest activity was observed in isopropanol (log *p* value of .05), a more hydrophilic solvent than hexane (log *p* value of 3.5), the most hydrophobic solvent used. Appreciably high relative activities were also observed in all other hydrophilic solvents tested (methanol, log *p* −.76; ethanol, log *p* −.24; Acetone, log *p* −.23). On the other hand, ethyl acetate and dichloromethane almost completely inhibited lipase activity (Table 5).

Table 5. Effect of organic solvents on activity of *Ro*L-ZAC3.

Organic solvents	log *P*	Relative activity (%)
Methanol	−0.76	86.2 ± 1.6
Ethanol	−0.24	69.6 ± 7.8
Acetone	−0.23	65.5 ± 8.8
Isopropanol	0.05	100 ± 3.1
t-butanol	0.58	23.3 ± 4.5
Ethylacetate	0.64	5.4 ± 0.6
Dichloromethane	1.25	2.0 ± 0.1
n-Hexane	3.5	27.1 ± 5.6

The buffer in the reaction mixture was replaced with 20% solution of the organic solvent. The percentage activity for each organic solvent was determined relative to the activity obtained with isopropanol. log *P* = logarithm of partition coefficient. Values are means ± SD ($n = 3$).

Substrate specificity

Chain length specificity of *Ro*L-ZAC3 evaluated using *p*-nitrophenyl esters with acyl chain lengths ranging from C2 to C18 showed that *p*-nitrophenyl oleate (*p*NPO), a long chain monounsaturated fatty acid ester (C18), had the highest relative activity reaching about 130% (Figure 4) as the lipolytic activity decreased towards saturated fatty acid chains.

Effect of RoL-ZAC3 on natural oils

*Ro*L-ZAC3 showed broad fatty acid specificity as indicated by its varied rate of hydrolysis of different natural triacylglycerols. Castor oil showed the highest hydrolysis rate, followed by olive oil. In comparison, lemon and origanum oils were hydrolysed more slowly (Figure 5).

Circular dichroism (CD) analysis

The probe of the global conformational stability was first attempted through CD study via its secondary structure stability analysis. The CD wavelength scan in the far UV region (200–260 nm) at pH 8 revealed a curve with two negative bands (double minima) typical of an α/β-protein (Figure 6). As the wavelength reduced from 260 nm to 200 nm, there was an increase in the negative ellipticity, which is typical of intact secondary structure elements. suggesting an increase in secondary structure. At pH 5, positive ellipticity was seen around 222 nm and a reduction in the negative molar ellipticity of the double minima which

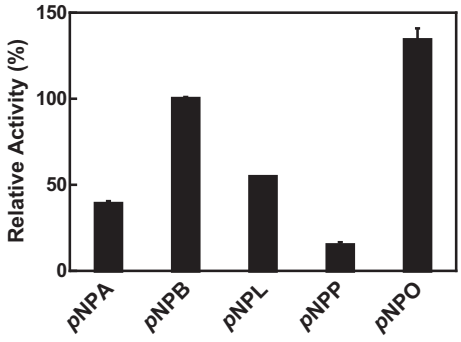

Figure 4. Substrate specificity of *Ro*L-ZAC3. This was done using 0.1% of the respective *p*-NP ester dissolved in isopropanol and then following the standard lipase assay. The percentage activities were determined relative to the reaction rate obtained with *p*NPB.

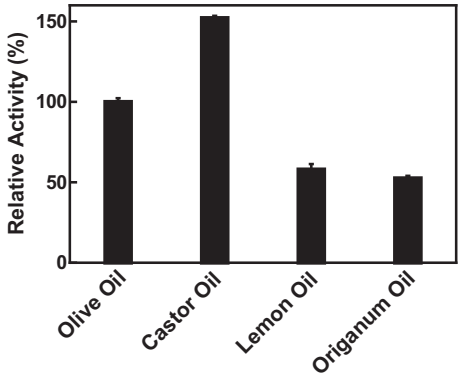

Figure 5. Effect of *Ro*L-ZAC3 on natural oils. This was done by titrimetric method. The reaction medium in 50 mM sodium phosphate buffer, pH 7 contained 10% (v/v) oil, 5% (w/v) gum arabic and 100 µL of the enzyme. This was incubated at 37 °C and terminated after 30 min. The released fatty acids were estimated by titration with 1 M NaOH. Data was expressed as percentage of value obtained for olive oil.

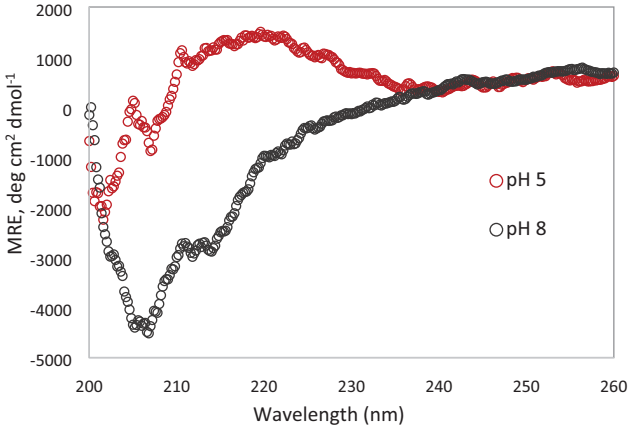

Figure 6. CD wavelength scan spectra at the far UV for *Ro*L-ZAC3 at pH 5 (white) and pH 8 (black). All scans were performed at 200–260 nm at a temperature of 25 °C. MRE, Mean residue ellipticity.

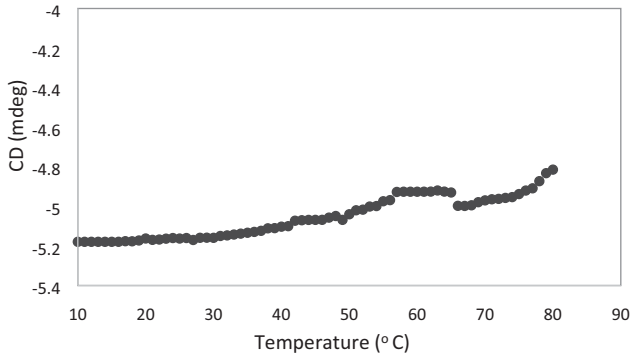

Figure 7. CD thermal scan (10–80 °C) of *Ro*L-ZAC3 run at a wavelength of 207 nm and at pH 8 to illustrate thermal unfolding of the enzyme.

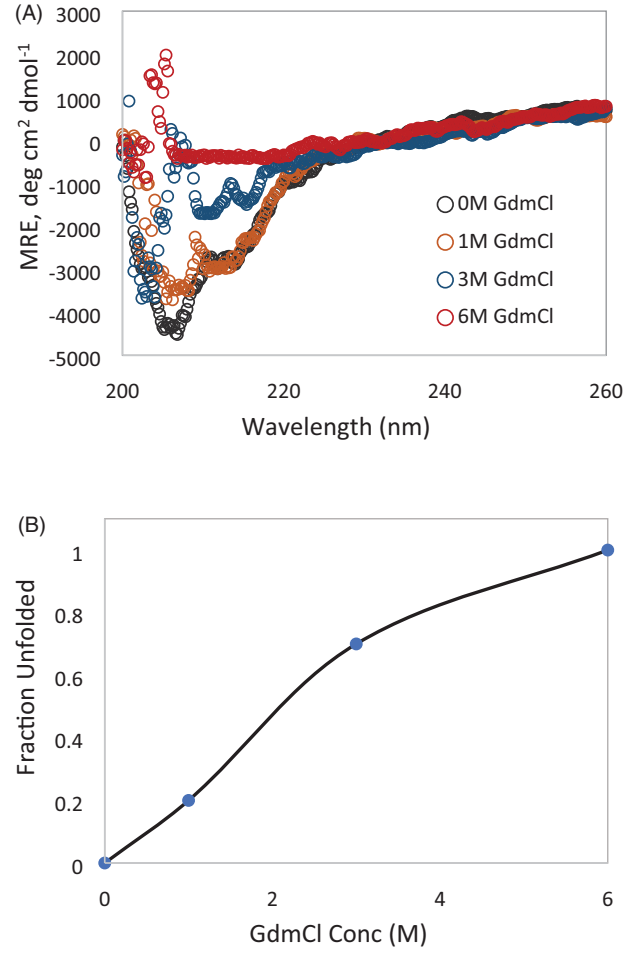

Figure 8. (A) CD spectra of *Ro*L-ZAC3 at 207 nm in the presence of guanidinium chloride of concentrations 0 M, 1 M, 3 M and 6 M. (B) Guanidinium chloride-induced unfolding of *Ro*L-ZAC3.

signifies a dramatic decrease in structure. For the CD thermal scan at a temperature range of 10–80 °C, there was not much difference between the negative ellipticity recorded at 10 °C and that recorded at 80 °C (Figure 7) which shows that very little unfolding occurred. Transforming the ellipticity (in mdeg) to

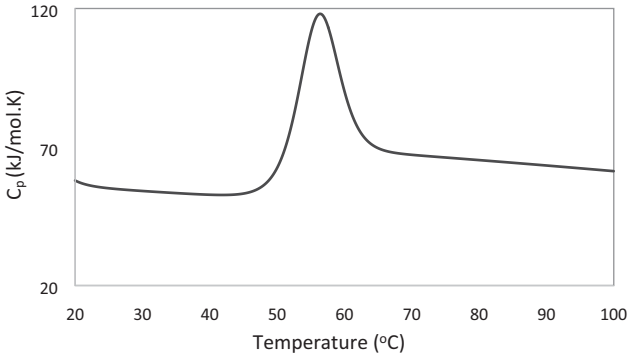

Figure 9. DSC thermogram of *Ro*L-ZAC3 at pH 8. The thermodynamic parameters are summarised in Table 6.

Table 6. Thermodynamic parameters of *Ro*L-ZAC3 deduced from DSC analysis.

	$t-T_m$ (°C)	ΔH_{cal} (kJ/mol)	ΔC_p (kJ/mol.K)
*Ro*LZAC3	55.5	444	19.4

fraction unfolded showed that there was barely any change in the ellipticity or fraction unfolded even as temperature approached 80 °C (Figure 7).

GdmCl caused unfolding in *Ro*L-ZAC3 (Figure 8(A)) as evidenced by changes in the structure of the CD spectra. At the 6 M GdmCl concentration, the double minima signature of secondary structure elements had completely disappeared. A low level (about 20%) of structure disruption was observed in the 1 M GdmCl – induced unfolding (Figure 8(A,B)) thus reflecting the stability of the enzyme at this concentration of GdmCl. At higher concentrations of GdmCl (3 M and 6 M), there is a considerable reduction of the regular conformation. This indicates that *Ro*L-ZAC3 secondary structure is not preserved at these higher concentrations of the denaturant.

Differential scanning calorimetry (DSC) analysis

The DSC thermogram (Figure 9) show baseline subtracted data of heat capacity plotted as a function of temperature. *Ro*L-ZAC3 exhibited single endothermic transition during unfolding and had a $t-T_m$ (tertiary structure unfolding temperature) of 55.5 °C. The protein heat capacity (C_p) was seen to be linear from 20 °C to 45 °C. The summary of the thermodynamic parameters is shown in Table 6.

Intrinsic tryptophan fluorescence analysis

Similar to DSC thermal scan that gave a $t-T_m$ of 55.5 °C, $t-T_m$ measured by fluorescence thermal scan was 50 °C (Figure 10(A,B)). There was a change in

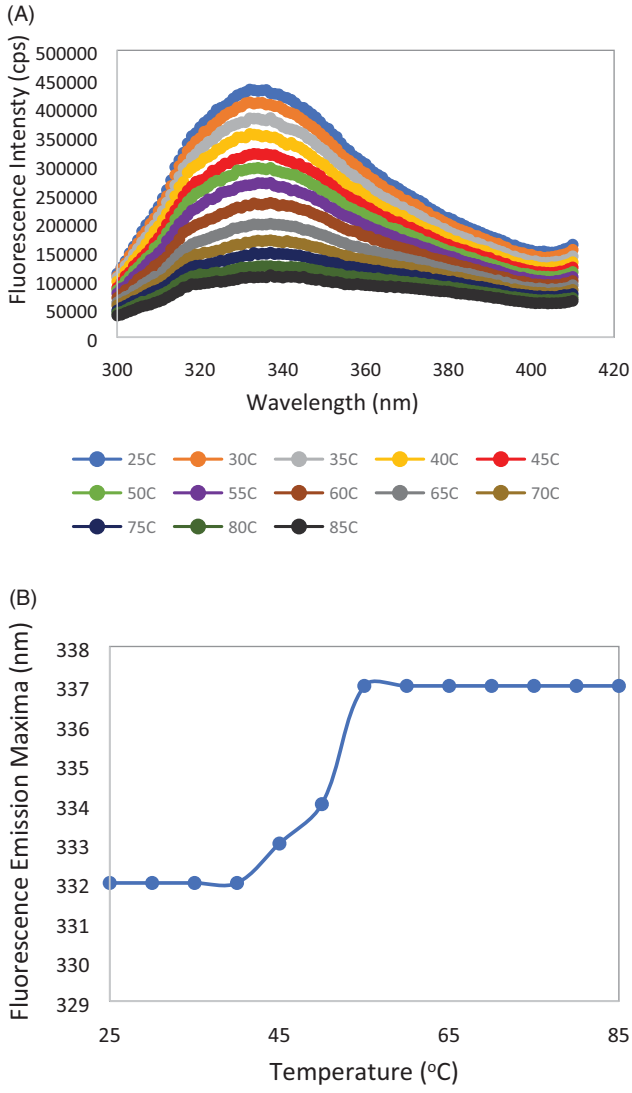

Figure 10. Temperature-induced unfolding of *Ro*L-ZAC3. (A) Fluorescence intensity as a function of temperature showing wavelength of maximum intensity (λ_{max}) at different temperatures thus revealing fluorescence of inner tryptophan residues. (B) temperature scans to identify thermal-induced unfolding of *Ro*L-ZAC3 and to determine the $t-T_m$.

fluorescence intensity (Figure 10(A)) as well as the significant shift in λ_{max} (Figure 10(B)), as temperature increased. There was a shift in λ_{max} from 332 nm at 25 °C to 337 nm at 55 °C and it remained at 337 nm even at 85 °C with concurrent decrease in fluorescence intensity.

Dynamic light scattering (DLS) analysis

Figure 11 shows the aggregation temperature (T_{agg}) which indicates the onset of aggregation. The molecules have a likelihood to begin to aggregate at this temperature. The T_{agg} was 50 °C for *Ro*L-ZAC3. The aggregates were not physically observed likely

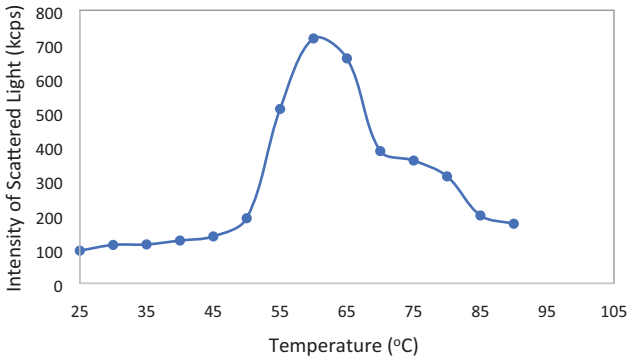

Figure 11. DLS analysis showing thermal induced aggregation of *Ro*L-ZAC3.

because they were at the nanoscale and could not be observed physically and/or only a small population of the protein molecules were involved. The T_{agg} obtained in the DLS study was close to and correlates the T_{opt} and the $t - T_m$ obtained by fluorescence and DSC analyses.

Discussion

*Ro*L-ZAC3 was extracellularly produced by the fungus, *Rhizopus oryzae* ZAC3, which was isolated from a palm oil contaminated soil, and the enzyme was purified by ultrafiltration and ion exchange chromatography. The distinct band from SDS-PAGE (Figure 1) ascertained the purity of the enzyme. With a molecular weight of 15.8 kDa, *Ro*L-ZAC3 is considered a very small lipase. Complete purification and characterisation of very low molecular weight fungal lipases, such as this, is not very common.

Temperature-activity studies provide an insight into the active site stability. Disruptions to the local active site structure can lead to loss of enzyme activity (Shirke et al. 2018). The T_{opt} value of 55 °C (Figure 2(A)) for the substrate (*p*NPB) is a good indicator of the stability of the active site or a decrease in the rigidity of the active site, improving traffic into and out of the active site and/or flexibility necessary for catalysis. The decline in enzyme activity beyond 55 °C, and the almost complete loss in activity at 85 °C were likely due to thermal-induced denaturation. Lipases purified from other sources showed optimum temperature around 35–55 °C; *Rhizopus oryzae,* 35 °C (Hiol et al. 2000), *Rhizopus* strain JK-1, 40 °C (Kantak and Prabhune 2012) and *Streptomyces rimosus* R6-554W, 55 °C (Abramić et al. 1999).

The thermal inactivation observed at very high temperature is a form of local unfolding (initiated as temperature rises above the T_{opt} and/or as time increases) which precedes the eventual loss of tertiary structure. The thermostability exhibited by *Ro*L-ZAC3 (Figure 2(B)) is quite promising. In comparison with other lipases purified from various *Rhizopus* species, *Ro*L-ZAC3 is relatively stable and appears to show better thermostability than some reported lipases. In thermal stability study of *Rhizopus chinensis* lipase by Sun et al. (2009), residual activity reduced to 55% after incubation at 50 °C for 60 min. Although, *Rhizopus oryzae* lipase by Hiol et al. (2000) retained about 65% of its activity after incubation at 45 °C for 30 min, however, all activity was lost following incubation at 50 °C for 30 min. At a specific operating temperature, a high value of the half-life is desired and beneficial for industrial applications (Shirke et al. 2016). Thus, the higher the $t_{1/2}$, the less prone the enzyme is to thermal denaturation. The high $t_{1/2}$ of *Ro*L-ZAC3 (Table 2) bears more relevance when compared with other fungal lipases at the same operating temperature. Free *Ro*L-ZAC3 displayed a $t_{1/2}$ of 2.1 h at 60 °C, unlike free *Candida rugosa* lipase which exhibited a half-life of 18 min at 60 °C while its immobilised form on cellulose nanocrystals had a half-life of 2 h at 60 °C (Kim et al. 2015).

*Ro*L-ZAC3 retained higher activity at slightly alkaline pH (Figure 3(A)). Enzyme activity and stability is strongly influenced by pH. Changes in pH cause changes in amino acid protonation state, which in turn greatly alter the spatial arrangements within the protein structure, as well as electrostatic interactions (Horng et al. 2005). As there are shifts in pH, it leads to changes in the state of protonation of active site residues, thus having effects on secondary and tertiary structure stability and leading not only to conformational changes but also changes in protein structure and activity. The enzyme was stable in slightly alkaline pH range of 7–8.5 over the 1 h incubation period (Figure 3(B)). Similar stability profile was observed in *Rhizopus oryzae* strain isolated from palm fruit, pH 7–8.5 (Hiol et al. 2000). Alkaline lipases, such as obtained in this study, offer promising prospect in bio-based industries such as detergent and textile industries.

The kinetic parameters tell the performance characteristics of the enzyme. The K_m gives an indication of the affinity of *Ro*L-ZAC3 for *p*NPB (Table 3). Comparison with other small lipases in literature may not be simple because the kinetic parameters were expressed in different units and in most cases, different substrates were used. Lipase from *Geobacillus stearothermophilus* AH22 showed a K_m and V_{max} of 0.02 mM and 1.03 U/mg respectively when pNPB was used as substrate (Ekinci et al. 2016) while *Rhizomucor*

miehei lipase had a K_m and V_{max} of 1.13 mM and 86.2 μM/min respectively (Tako et al. 2017) when *p*-nitrophenyl palmitate (*p*NPP) was used as substrate. While K_m obtained in this study (0.19 ± 0.02 mM) was higher than that obtained for *Geobacillus stearothermophilus* AH22 lipase which also utilised *p*NPB as substrate, the K_m was however about six times lower and V_{max} was about 1.28 times higher than values obtained for *Rhizopus oryzae* NRRL 1526 lipase, which utilised *p*NPP as substrate (Tako et al. 2017). A low K_m and high V_{max} indicates that the enzyme has a relatively higher affinity for its substrate and hydrolyses it better than its counterparts with a higher K_m.

If a heavy metal such as Hg^{2+} causes significant or complete inactivation of an enzyme, it may be an implication that thiol groups are necessary for adequate enzyme function (Tako et al. 2017). It is important to state that buffers have an influence on the chemical speciation of certain metals and heavy metal phosphates generally have very low solubility in aqueous medium and may sometimes precipitate out. Heavy metals react with sulfhydryl groups of enzymes and may cause inhibition of enzyme catalysis if an essential cysteine residue is involved (Reynolds et al. 1993). This correlates the poor lipase activity observed with Hg^{2+} in this study (Table 4). However, because only about 50% inhibition was observed at all three concentrations of Hg^{2+}, it suggests that the cysteine involved in the heavy metal binding may not be an essential residue that is key to catalysis. Similar to what was observed in this study, Na^+ ions showed similar stimulatory effects on lipase from *Rhizomucor miehei* (Tako et al. 2017). According to Noel and Combes (2003), the enzyme conformation is stabilised by the Na^+ ions by strengthening the integrity of the active site and thereby enhancing enzyme activity. The possibility that the 50 mM sodium phosphate buffer had an additive effect on the high activity observed with Na^+ ions cannot be ruled out. Woehl and Dunn (1995) proposed two possible mechanisms to explain the role of monovalent metal ions in enzyme catalysis: either the metal ion plays a static structural role whereby it activates and stabilises the catalytically active conformation of the enzyme by simply binding to it or the metal ion plays a dynamic role whereby it binds selectively to ensure that protein conformational transition takes place which is necessary for the complementarity between the structure of an activated complex and the enzyme site. The high activity at increased Ca^{2+} concentrations of 10 and 20 mM correlated the finding demonstrated by Kambourova et al. (2003) that Ca^{2+} ions enhance microbial lipase activity. Literature review has revealed that certain lipases, such as that from *Burkholderia glumae* (El-Khattabi et al. 2003) have a Ca^{2+}-binding site. Two conserved aspartate residues very close to the active site form this binding site. According to Kambourova et al. (2003) lipase activity enhancement by Ca^{2+} is mainly because during hydrolysis, insoluble ion salts of fatty acids form, thus product inhibition is avoided. Alternatively, the increase in enzyme activation observed as Ca^{2+} ion concentration increased may be as a result of a higher Ca^{2+} ion concentration inducing a conformational change of the enzyme structure to a more active form. The Ca^{2+} ions may form salt bridges between two COO^- groups of acidic amino acids that might have better stabilised the enzyme structure and caused the increase in activity observed.

All organic synthesis processes require enzymes to remain active and stable in most organic solvents. Enzyme stability in aqueous media largely differ from its stability in organic media mainly because organic media has low water content and that leads to increased conformational rigidity of the enzyme. *Ro*L-ZAC3 displayed varying stabilities in the different hydrophobic and hydrophilic organic solvents tested (Table 5). The log *p* value is used to distinguish organic solvents on the basis of their hydrophilic or hydrophobic nature. The higher the log *p* value, the more hydrophobic the organic solvent and vice-versa (Imanparast et al. 2018). According to Doukyu and Ogino (2010), microbial lipases show greater activity in hydrophobic solvents than in hydrophilic solvents, even though the contrary was observed in this study. Similar result to what was obtained in this study was observed in lipase from *Actinomadura sediminis* UTMC 2870 which showed stability in hydrophilic solvents with low log *p* values (Imanparast et al. 2018). Likewise, in *Rhizomucor miehei* NRRL 5282 and *Rhizopus oryzae* NRRL 1526 (Tako et al. 2017), the lipase remained stable in 20% (v/v) methanol and ethanol. A possible explanation for the higher activity observed in hydrophilic solvents (known to strip crucial water off enzyme molecules) is that the enzyme is able to retain high water content (high enough to remain catalytically active) probably because the essential water/hydration shell is tightly bound to the enzyme molecule (Klibanov 1989). It is also possible that activity varied due to the loss of hydrophobic pressure in protein folding and likely less structure than rigidity. On the other hand, Doukyu and Ogino (2010) put forward a number of factors to explain enzyme activity loss seen in certain organic media.

The enzyme deactivation in hydrophobic organic media occurs when the protein molecule hydrophobic core is disrupted due to a change of medium hydrophobicity. Unlike water, anhydrous solvents may render enzymes less active due to restricted and decreased conformational flexibility causing rigidity of the enzyme conformation (Doukyu and Ogino 2010). As hydrophobic solvents do not strip off essential water on the enzyme molecules which is crucial for the maintenance of enzyme structure and function, they sometimes help to promote enzymatic reactions in anhydrous solvents (Klibanov 1997).

There was a decrease in the rate of hydrolysis as chain length of the fatty acid esters increased from 4 to 12 to 16 carbon atoms. However, *p*-nitrophenyl oleate, *p*NPO (C18:1), a monounsaturated fatty acid ester was an exception and did not follow this pattern. It had the highest relative activity as the lipolytic activity decreased towards saturated fatty acid chains (Figure 4). Since hydrolysis by hydrolases such as lipases occur in heterogeneous systems, this exception by *p*NPO could be due to the orientation of the molecule at the oil/water interface (which would influence enzyme-substrate association) or due to enzyme-substrate specificity or due to both reasons. Chain length specificity varies generally between C8 and C18 acids for lipases from filamentous fungi while lipases from zygomycete show maximum activity towards medium (C6–C12) or long chain acids (C14–C20) though high reaction specificity towards C2 to C6 acids is displayed by some of them (Yu et al. 2009).

*Ro*L-ZAC3 activity towards different natural triglycerides (vegetable oils) further revealed some important preferences in terms of substrate specificity. Plant oils are a mixture of triacylglycerols with different fatty acid chain lengths. The highest hydrolysis rate was seen in castor oil, followed by olive oil (Figure 5). Castor oil is composed majorly of about 85–90% of ricinoleic acid, a monounsaturated fatty acid with a hydroxyl functional group which makes it more polar than its counterparts. Olive oil, on the other hand is composed of 55–83% oleic acid (McKeon 2016), which is also monounsaturated and having 18 carbon atoms just as ricinoleic acid. This is consistent with the chain length specificity results obtained in this study in which *p*NPO gave the highest hydrolytic activity. The results here further confirm the enzyme has preference for long chain, monounsaturated fatty acid esters. Its ability to hydrolyse both natural triglycerides and synthetic aryl esters shows that it has potential application in large scale fat hydrolysis which can be further investigated.

The CD structure of *Ro*L-ZAC3 at pH 5 resembles that of a random coil (Figure 6). *Ro*L-ZAC3 retained only about 50% of its structure at pH 5 relative to pH 8 as evidenced by the reduced signal intensity. This implies that some degree of its original secondary structure had been lost at the acidic pH of 5. As denaturation sets in, some secondary structure elements should normally deplete. This correlates the result from the effect of pH (Figure 3(A)) where over 90% of *Ro*L-ZAC3 activity had been lost at pH 5 compared to the activity at optimum pH 8. This appears reasonable because according to Shashidhara and Gaikwad (2010), at very acidic pH, all side chains that are ionisable become protonated resulting in a charge-charge repulsion that causes loosening of side chain packing and eventually hydrophobic residues become exposed to the solvent leading to loss of secondary structure.

The CD thermal scan should normally reveal the melting/unfolding temperature (T_m), which is usually the midpoint of the thermal transition curve. During the thermal unfolding monitored by CD in this study, no clear thermal-induced transitions occurred up to 80 °C (Figure 7), thus the apparent T_m could not be ascertained from the CD. Since CD (at far UV wavelengths) assesses majorly secondary structure elements, the implication of this result is that *Ro*L-ZAC3 displayed substantial secondary structure stability. Similar finding was reported by Shirke et al. (2018) in which no thermal transition was observed in glycosylated leaf and branch compost cutinase (LCC) up to 95 °C following thermal unfolding studies by CD. One possible explanation for T_m not observed in CD analysis is that as temperature increased up to and above the T_{opt}, some structural changes attributed to denaturation might have occurred close to the active site, which would normally not be reflected in the CD spectrum. CD spectra only reflect secondary structure stability or otherwise. The T_{opt} recorded in this study was 55 °C, yet T_m was not ascertained even at 80 °C by CD. Sulaiman et al. (2012) also reported a T_{opt} of 50 °C and T_m of 86 °C for non-glycosylated leaf and branch compost cutinase (LCC-NG) which was considered a very wide gap. With the large difference between the T_{opt} (an indication of local active site stability) and T_m (an indication of global conformational stability), another unfolding experiment technique was necessary to further probe the global conformational stability via DSC and Intrinsic tryptophan fluorescence analysis on the tertiary structure. It is important to state that one limitation of CD analysis is that it may

not detect minute structural changes that can cause activity loss (Shirke et al. 2017).

Prior to analysis by fluorescence, it was important to confirm the secondary structure stability implied from the CD results. Samples were incubated overnight with different concentrations of guanidinium chloride (GdmCl) followed by CD analysis. As the concentration of GdmCl was increased from 1 M to 3 M, transition from native to unfolded state was observed (Figure 8(A)). The GdmCl-denaturation data is an indication that *Ro*L-ZAC3 underwent complete loss of its α-helical component and changes in other secondary structural elements at 6 M GdmCl. The concentration at the transition midpoint (C_m) is the GdmCl concentration where 50% of the protein is unfolded (He et al. 2009). This was about 2.2 M for *Ro*L-ZAC3. Brito e Cunha et al. (2019) studied the secondary structural stability of commercial (CalB) and recombinant (LipB) lipase B from *Candida Antarctica* in the presence of urea and GdmCl at different concentrations. A gradual loss of secondary structure began above 1 M and 3 M urea concentration for LipB and CalB respectively. Some secondary structural elements were still maintained even at a high concentration of 8 M by both enzymes. When GdmCl was used as the chaotropic agent, a prominent structure loss was observed in both LipB and CalB, even at a low GdmCl concentration of 1 M. At 3 M GdmCl, complete denaturation of both enzymes was observed (Brito e Cunha et al. 2019). At 1 M GdmCl, *Ro*L-ZAC3 still maintained a significant percentage of its native structure, at 3 M GdmCl, only about 28% of its structure is preserved while at 6 M GdmCl there was complete loss of structure (Figure 8(A)). Literature has proposed that chaotropic agents may act by interacting directly with the polar side chains and the protein backbone or by interacting with water causing perturbations in the water solvation (O'Brien et al. 2007). Studies have also shown that lower GdmCl concentrations than urea are needed to reach the protein unfolding midpoint because GdmCl is more efficient in protein solvation causing salt bridges and hydrogen bonds to rupture (O'Brien et al. 2007).

For the DSC analysis (Figure 9), the linear heat capacity from 20 °C to 45 °C implied that no domains or regions displayed any significant degree of unfolding before the commencement of the actual thermal transition/heat denaturation at around 50 °C. Loss of tertiary structure is a cooperative process usually associated with a large enthalpy and entropy change. The $t - T_m$ obtained from the analysis was 55.5 °C, which is very close to the T_{opt} of 55 °C; ΔH_{cal} (calorimetric enthalpy) of 444 kJ/mol and ΔC_p (change in heat capacity at constant pressure) of 19.4 kJ/mol.K (Table 6). ΔC_p is a measure of the extent to which non-polar groups are exposed to water (Privalor 1979). A positive ΔC_p implies solvation of the unfolded polar groups of the protein (Richardson and Makhatadze 2004) and solvation of the polar groups may mean difficulty in the refolding of groups back to the tertiary structure. The thermal unfolding of lipase from *Pseudomonas fluorescens* had a ΔC_p of 4 kJ/mol.K (Makhzoum et al. 1993) which is comparatively lower than 19.4 kJ/mol.K obtained for RoL-ZAC3. A high C_p means that the process of unfolding is a slow one.

While CD gives information on 2° structure unfolding, DSC and fluorescence thermal analysis give information on 3° structure unfolding. Temperature was used to perturb and monitor changes in the 3° structure of *Ro*L-ZAC3 via intrinsic tryptophan fluorescence analysis. Hydrophobic side chains are exposed when unfolding or partial loss of 3° structure occurs and this exposure may sometimes contribute to aggregation. Tryptophan residues (selectively excited at 295 nm) when buried, show an emission maxima (λ_{max}) around 330 nm, which on solvent exposure, shifts to a longer wavelength, sometimes greater than 340 nm. The fluorescence intensity change (Figure 10(A)) and the significant shift in λ_{max} (Figure 10(B)) as temperature was raised, was an indication that a change had occurred in the local tryptophan environment of *Ro*L-ZAC3 suggesting thermal unfolding at the 3° structure level. The red shift in λ_{max} from 332 nm at 25 °C to 337 nm at 55 °C with simultaneous decrease in fluorescence intensity suggests that some of the tryptophan residues of the enzyme had been exposed to the solvent of the surrounding environment (Castro-Ochoa et al. 2005). In other words, the tryptophan residues must have moved to a more polar environment from the non-polar interior. The decrease in fluorescence intensity implied that the fluorescence of the tryptophan residues in the denatured enzyme had been greatly quenched. Upon unfolding, a protein loses many of the interactions that maintain its native structure. Decrease in the rigidity of the side chains also set in as unfolding occurs. As the CD thermal scan did not reveal unfolding of the protein, it may imply that Trp residues are not directly involved in maintaining the protein secondary structure.

Aggregation studies were carried out using DLS analysis. Protein aggregation sets in after unfolding, following exposure of more hydrophobic surface area (Yan et al. 2003). As proteins aggregate, the aggregates scatter light to different intensities, depending

on the sizes of the aggregates. Scattered light intensity was monitored as a function of temperature. A sharp increase in scattered light intensity, as temperature increased, marked the onset of aggregation (Figure 11). Aggregation tendencies are most likely due to enhanced hydrophobic interactions following partial disruption/loss of tertiary structure. With a T_{opt} of 55 °C (local active site unfolding temperature), $t - T_m$ of 55 °C (measured by DSC) and 50 °C (measured by fluorescence analysis), T_{agg} of 50 °C (measured by DLS thermal scan) and CD $T_m > 80$ °C (a clear thermal-induced 2° structure unfolding was not observed up to 80 °C), it can be seen that these observations are in agreement with a proposed unfolding mechanism by Shirke et al. (2018) that tertiary structure loss starts at the fluorescence-determined unfolding temperature.

Conclusion

An unusually low molecular weight lipase from *Rhizopus oryzae* ZAC3 was purified and extensively characterised. *Ro*L-ZAC3 showed optimum activity at 55 °C and pH 8. It exhibited enzymatic activity on a broad range of substrates and was stable over a wide range of temperature and pH. Its stability in organic solvents with low log*P* values such as methanol and ethanol suggest its potential applications in transesterification reactions. It also displayed impressive secondary structure stability. Based on the characterisation results and the benefits inherent in low molecular weight lipases, *Ro*L-ZAC3 has interesting potential in industrial applications.

Acknowledgements

Structural studies were carried out at the Center for Biotechnology and Interdisciplinary Studies (CBIS), Rensselaer Polytechnic Institute (RPI), Troy, New York. We acknowledge the Analytical Biochemistry Core Facility of CBIS for the support in carrying out the biophysical aspect of this work.

Disclosure statement

No potential conflict of interest was reported by the author(s).

ORCID

Femi K. Agboola http://orcid.org/0000-0001-6023-2872

References

Abramić M, Leščić I, Korica T, Vitale L, Saenger W, Pigac J. 1999. Purification and properties of extracellular lipase from *Streptomyces rimosus*. Enzyme Microb Technol. 25(6): 522–529.

Ayinla ZA, Ademakinwa AN, Agboola FK. 2017. Studies on the optimization of lipase production by *Rhizopus* sp. ZAC3 isolated from the contaminated soil of a palm oil processing shed. J Appl Biol Biotechnol. 5(2):30–37.

Brito e Cunha DA, Bartkevihi L, Robert JM, Cipolatti EP, Ferreira ATS, Oliveira DMP, Gomes-Neto F, Almeida RV, Fernandez-Lafuente R, Freire DMG, et al. 2019. Structural differences of commercial and recombinant lipase B from *Candida antarctica*: an important implication on enzymes thermostability. Int J Biol Macromol. 140:761–770.

Castro-Ochoa LD, Rodriguez-Gomez C, Valerio-Alfaro G, Ros RO. 2005. Screening, purification and characterization of the thermoalkalophilic lipase produced by *Bacillus thermoleovorans* CCR11. Enzyme Microb Technol. 37(6):648–654.

Dobrev G, Zhekova B, Nedelcheva P, Chochkov R, Krastanov A. 2011. Characterization of crude lipase from *Rhizopus arrhizus* and purification of multiplicity forms of the enzyme. Biotechnol Biotechnol Equip. 25(1):2295–2300.

Doukyu N, Ogino H. 2010. Organic solvent-tolerant enzymes. Biochem Eng J. 48(3):270–282.

Ekinci AP, Dinçer B, Baltaş N, Adıgüzel A. 2016. Partial purification and characterization of lipase from *Geobacillus stearothermophilus* AH22. J Enzyme Inhib Med Chem. 31(2):325–331.

El-Khattabi M, Van Gelder P, Bitter W, Tommassen J. 2003. Role of the calcium ion and the disulfide bond in the *Burkholderia glumae* lipase. J Mol Catal B Enzym. 22(5–6): 329–338.

He GJ, Zhang A, Liu WF, Cheng Y, Yan YB. 2009. Conformational stability and multistate unfolding of poly(A)-specific ribonuclease. FEBS J. 276(10):2849–2860.

Hiol A, Jonzo MD, Rugani N, Druet D, Sarda L, Comeau LC. 2000. Purification and characterization of an extracellular lipase from a thermophilic *Rhizopus oryzae* strain isolated from palm fruit. Enzyme Microb Technol. 26(5–6):421–430.

Horng JC, Cho JH, Raleigh DP. 2005. Analysis of the pH-dependent folding and stability of histidine point mutants allows characterization of the denatured state and transition state for protein folding. J Mol Biol. 345(1):163–173.

Imanparast S, Hamedi J, Faramarzi MA. 2018. Enzymatic esterification of acylglycerols rich in omega-3 from flaxseed oil by an immobilized solvent-tolerant lipase from *Actinomadura sediminis* UTMC 2870 isolated from oil-contaminated soil. Food Chem. 245:934–942.

Kambourova M, Kirilova N, Mandeva R, Derekova A. 2003. Purification and properties of thermostable lipase from a thermophilic *Bacillus stearothermophilus* MC7. J Mol Catal B Enzym. 22(5–6):307–313.

Kantak J, Prabhune A. 2012. Characterization of smallest active monomeric lipase from novel *Rhizopus* strain: application in transesterification. Appl Biochem Biotechnol. 166(7):1769–1780.

Kim HJ, Park S, Kim SH, Kim JH, Yu H, Kim HJ, Hyung HY, Yung-Hun JK, Kan YE, Kim YH, Lee SH. 2015. Biocompatible cellulose nanocrystals as supports to immobilize lipase. J Mol Catal B Enzym. 122:170–178.

Kishore D, Kundu S, Kayastha AM. 2012. Thermal, chemical and pH induced denaturation of a multimeric β-galactosidase reveals multiple unfolding pathways. PLoS One. 7(11):e50380.

Klibanov A. 1989. Enzymatic catalysis in anhydrous organic solvents. Trends Biochem Sci. 14(4):141–144.

Klibanov AM. 1997. Why are enzymes less active in organic solvents than in water? Trends Biotechnol. 15(3):97–101.

Krusemark CJ, Frey BL, Smith LM, Belshaw PJ. 2011. Complete chemical modification of amine and acid functional groups of peptides and small proteins. Methods Mol Biol. 753:77–91.

Laemmli UK. 1970. Cleavage of structural proteins during the assembly of the head of bacteriophage T4. Nature. 227(5259):680–685.

Lee D-W, Kim H-W, Lee K-W, Kim B-C, Choe E-A, Seung Lee H, Kim D-S, Pyun Y-R. 2001. Purification and characterization of two distinct thermostable lipases from the gram-positive thermophilic bacterium *Bacillus thermoleovorans* ID-1. Enzyme Microb Technol. 29(6–7):363–371.

Lineweaver H, Burk D. 1934. The determination of enzyme dissociation constants. J Am Chem Soc. 56(3):658–666.

Makhzoum A, Owusu RK, Knapp JS. 1993. The conformational stability of a lipase from a psychrotrophic *Pseudomonas fluorescens*. Food Chem. 46(4):355–359.

Mase T, Matsumiya Y, Akiba T. 1995. Purification and characterization of a new lipase from *Fusarium* sp. YM-30. Biosci Biotechnol Biochem. 59(9):1771–1772.

McKeon TA. 2016. Castor (*Ricinus communis* L.). In: McKeon TA, Hayes DG, Weselake RJ, Hildebrand DF, editors. Industrial oil crops. Urbana (IL): AOCS Press; Waltham (MA): Elsevier Inc.; p. 75–112.

Mehta A, Bodh U, Gupta R. 2017. Fungal lipases: a review. J Biotech Res. 8(1):58–77.

Noel M, Combes D. 2003. *Rhizomucor miehei* lipase: differential scanning calorimetry and pressure/temperature stability studies in presence of soluble additives. Enzyme Microb. Technol. 33(2–3):299–308.

O'Brien EP, Dima RI, Brooks B, Thirumalai D. 2007. Interactions between hydrophobic and ionic solutes in aqueous guanidinium chloride and urea solutions: lessons for protein denaturation mechanism. J Am Chem Soc. 129:7346–7353.

Pimentel MCB, Leao ABF, Melo EHM, Ledingham WM, Lima Filho JL, Sivewright M, Kennedy JF. 2007. Immobilization of *Candida rugosa* lipase on magnetized Dacron: kinetic study. Artif Cells Nanomed Biotechnol. 35(2):221–235.

Privalor PL. 1979. Stability of proteins: small globular proteins. Adv Protein Chem. 33:167–241.

Rabbani G, Ahmad E, Zaidi N, Fatima S, Khan RH. 2012. pH-Induced molten globule state of *Rhizopus niveus* lipase is more resistant against thermal and chemical denaturation than its native state. Cell Biochem Biophys. 62(3):487–499.

Reynolds LJ, Hughes LL, Louis AI, Kramer RM, Dennis EA. 1993. Metal ion and salt effects on the phospholipase A2, lysophospholipase and transacylase activities of human cytosolic phospholipase A2. Biochim Biophys Acta. 1167(3):272–280.

Richardson JM, Makhatadze GI. 2004. Temperature dependence of the thermodynamics of helix-coil transition. J Mol Biol. 335(4):1029–1037.

Salihu A, Alam MZ. 2012. Production and applications of microbial lipases: A review. Sci Res Essays. 7(30): 2667–2677.

Shashidhara KS, Gaikwad SM. 2010. Conformational and functional transcription in class II α-mannoside from *Aspergillus fischeri*. J Fluoresc. 20(4):827–836.

Shirke AN, Basore D, Butterfoss GL, Linhardt RJ, Bonneau R, Bystroff C, Gross R. 2016. Toward rational thermostabilization of *Aspergillus oryzae* cutinase: Insights into catalytic and structural stability. Proteins. 84(1):60–72.

Shirke AN, Su A, Jones JA, Butterfoss GL, Koffas MAG, Kim JA, Gross RA. 2017. Comparative thermal inactivation analysis of *Aspergillus oryzae* and *Thiellavia terrestris* cutinase: role of glycosylation. Biotechnol Bioeng. 114(1):63–73.

Shirke AN, White C, Englaender JA, Zwarycz A, Butterfoss GL, Linhardt RJ, Gross R. 2018. Stabilizing leaf and branch compost cutinase (LCC) with glycosylation: mechanism and effect on PET hydrolysis. Biochemistry. 57(7): 1190–1200.

Sirisha E, Rajasekar N, Narasu ML. 2010. Isolation and optimization of lipase producing bacteria from oil-contaminated soils. Adv Biol Res. 4(5):249–252.

Smith PK, Krohn RI, Hermanson GT, Mallia AK, Gartner FH, Provenzano MD, Fujimoto EK, Goeke NM, Olson BJ, Klenk DC. 1985. Measurement of protein using bicinchoninic acid. Anal Biochem. 150(1):76–85.

Sulaiman S, Yamato S, Kanaya E, Kim J–J, Koga Y, Takano K, Kanaya S. 2012. Isolation of a novel cutinase homolog with polyethylene terephthalate-degrading activity from leaf-branch compost by using a metagenomic approach. Appl Environ Microbiol. 78(5):1556–1562.

Sun SY, Xu Y, Wang D. 2009. Novel minor lipase from *Rhizopus chinensis* during solid-state fermentation: biochemical characterization and its esterification potential for ester synthesis. Bioresour Technol. 100(9):2607–2612.

Tako M, Kotogan A, Papp T, Kadaikunnan S, Alharbi NS, Vagvolgyi C. 2017. Purification and properties of extracellular lipases with transesterification activity and 1,3-regioselectivity from *Rhizomucor miehei* and *Rhizopus oryzae*. J Microbiol Biotechnol. 27(2):277–288.

Vorderwulbecke T, Kieslich K, Erdmann H. 1992. Comparison of lipases by different assays. Enzyme Microb Technol. 14(8):632–639.

Woehl EU, Dunn MF. 1995. The roles of Na^+ and K^+ in pyridoxal phosphate enzyme catalysis. Coord Chem Rev. 144: 147–197.

Yan YB, Wang Q, He HW, Hu XY, Zhang RQ, Zhou HM. 2003. Two-dimensional infrared correlation spectroscopy study of sequential events in the heat-induced unfolding and aggregation process of myoglobin. Biophys J. 85(3): 1959–1967.

Yu XW, Wang LL, Xu Y. 2009. *Rhizopus chinensis* lipase: gene cloning, expression in *Pichia pastoris* and properties. J Mol Catal B Enzym. 57(1–4):304–311.